Design and validation of the RiceWrist-S exoskeleton for robotic rehabilitation after incomplete spinal cord injury

Ali Utku Pehlivan, Fabrizio Sergi, Andrew Erwin, Nuray Yozbatiran, Gerard E. Francisco and Marcia K. O'Malley

Robotica / Volume 32 / Special Issue 08 / December 2014, pp 1415 - 1431
DOI: 10.1017/S0263574714001490, Published online: 20 June 2014

Robotica (2014) volume 32, pp. 1415–1431. © Cambridge University Press 2014
doi:10.1017/S0263574714001490

Design and validation of the RiceWrist-S exoskeleton for robotic rehabilitation after incomplete spinal cord injury

Ali Utku Pehlivan†,*, Fabrizio Sergi†‡, Andrew Erwin†, Nuray Yozbatiran§, Gerard E. Francisco§ and Marcia K. O'Malley†

†*Mechatronics and Haptic Interfaces Laboratory, Department of Mechanical Engineering, Rice University, Houston, TX 77005*
‡*Department of PM& R, Baylor College of Medicine, Houston, TX 77030*
§*Department of PM& R and UTHealth Motor Recovery Lab, University of Texas Health Science Center at Houston, TX 77030*

(Accepted May 19, 2014. First published online: June 20, 2014)

SUMMARY
Robotic devices are well-suited to provide high intensity upper limb therapy in order to induce plasticity and facilitate recovery from brain and spinal cord injury. In order to realise gains in functional independence, devices that target the distal joints of the arm are necessary. Further, the robotic device must exhibit key dynamic properties that enable both high dynamic transparency for assessment, and implementation of novel interaction control modes that significantly engage the participant. In this paper, we present the kinematic design, dynamical characterization, and clinical validation of the RiceWrist-S, a serial robotic mechanism that facilitates rehabilitation of the forearm in pronation-supination, and of the wrist in flexion-extension and radial-ulnar deviation. The RiceWrist-Grip, a grip force sensing handle, is shown to provide grip force measurements that correlate well with those acquired from a hand dynamometer. Clinical validation via a single case study of incomplete spinal cord injury rehabilitation for an individual with injury at the C3-5 level showed moderate gains in clinical outcome measures. Robotic measures of movement smoothness also captured gains, supporting our hypothesis that intensive upper limb rehabilitation with the RiceWrist-S would show beneficial outcomes.

KEYWORDS: Robot dynamics; Exoskeletons; Robotic rehabilitation; Human-robot interaction.

1. Introduction

Neurological impairments, such as stroke and spinal cord injuries, affect a significant portion of the population, and research findings show that intensive rehabilitation can induce neural plasticity, thereby affecting recovery of function and independence among these populations.[1–4] In the United States, about 795,000 people suffer a stroke each year. Stroke, the leading cause of long-term disability, has a significant social and economic impact with an estimated $38.6 billion annual cost.[5] Further, there are approximately 12,000 incidences of Spinal Cord Injury (SCI) in the United States each year,[6] with estimated total yearly direct and indirect costs of $14.5 billion and $5.5 billion, respectively.[7] Both of these neurological injuries give rise to significant upper limb motor impairment. Given the clear economical impact of these conditions, and owing to the beneficial effects of intensive physical therapy, interest in robotic rehabilitation has increased greatly in recent years. The potential for robotic devices to significantly impact therapy practices, and in turn functional recovery, is attributed to the

* Corresponding author. E-mail: aup1@rice.edu

fact that robotic devices can deliver this beneficial intensive rehabilitation in a more cost effective manner.[8]

Generally speaking, rehabilitation of patients affected by neurological lesions, including stroke and SCI, is intended to induce brain and spinal cord plasticity and to improve functional outcomes. In order to fulfill this goal, therapy must be intensive.[9] Robotic devices are well suited to offer consistent delivery of intensive therapy, coupled with the opportunity to perform objective and quantitative performance evaluation of patients using the vast sensor data inherently available in these robotic devices. Further, such objective assessment of therapeutic impact can be assessed throughout the course of therapy, giving the therapist and the patient a detailed and near real-time snapshot of motor impairment changes facilitated by the robotic device. This extensive assessment is typically not feasible with the clinical assessments and tests commonly used to assess efficacy of classical rehabilitation. Indeed, robotic devices are being increasingly included in rehabilitation protocols, and the results of clinical studies with both stroke,[8] and SCI patients[10] support this approach.

While robotic devices can clearly provide intensive and repetitive movement training, not every robotic device or therapy protocol has been shown to be capable of promoting plasticity-mediated recovery. In order to fulfill this goal, robotic therapy must engage the participant, which can be achieved by sharing control of movements with the subjects, through interaction controllers,[11] patient adaptive control modes,[12] or progressively resisting control modes.[13] In order to support these varied interaction modes, the design of the robotic device needs to exhibit specific properties such as low apparent inertia and friction, isotropic dynamic characteristics, and minimal backlash. These design features ensure that the device will be transparent to the subject during robotic assessment of motor coordination, where subjects backdrive the robotic device and motion data are recorded for analysis. Additionally, these design features facilitate the implementation of accurate interaction control algorithms.

Nearly all activities of daily living (ADL), such as eating, drinking, cleaning, and dressing, involve distal upper extremity movement and a certain level of manual dexterity. In order for a person who has suffered a stroke or SCI to regain the ability to perform these ADLs, effective rehabilitation of the upper limbs, especially the distal joints, is required. Consequently, a growing number of research groups have developed robotic devices for rehabilitation of the distal joints of the upper extremity. For example, Colombo *et al*. employ a one degree of freedom (DOF) wrist manipulator in conjunction with a two DOF elbow-shoulder manipulator in their clinical evaluation of stroke rehabilitation.[14] Although the wrist manipulator can apply large torque outputs, its actuation is limited only to wrist flexion/extension movements. The Arm Trainer[15] and Universal Haptic Drive (UHD)[16] are designed to actuate two out of three DOFs of human wrist for a given configuration. Both devices use geared transmissions, which can reduce the backdrivability of the device. Some of these limitations were addressed by Krebs *et al*. who developed a compact 3-DOF wrist robot.[17] Their system is capable of matching the complete range of motion (ROM) required for ADLs of the wrist by employing a differential gear mechanism, that provides the advantage of limiting the reflected inertia for flexion/extension (FE) and radial/ulnar deviation (RU), but introduces some friction and requires expensive, high-accuracy mechanical components. In a subsequent robot-aided stroke rehabilitation study, Squeri *et al*. proposed a new 3 DOF wrist robotic exoskeleton.[18] Although the design approximately covers the required ROM for wrist movement ADLs,[19] it is unclear how both the incorporation of gear drives and coupled movements between the actuator for wrist flexion/extension and the handle reflects on the backdrivability and transparency of the device, specifically in terms of friction and end point inertia.

In this paper, we present the RiceWrist-S (Fig. 1), a forearm-wrist robotic exoskeleton intended for stroke and SCI rehabilitation. The RiceWrist-S is designed to provide high torque output and cover the complete workspace of the human wrist. Such performance is achieved while also providing minimal friction, gravitational and inertial loading, by means of a cable drive transmission. The paper is structured as follows. In Section 2, we present the design and characterization of the RiceWrist-S, in conjunction with the details and rationale of design choices, and procedures and results of device characterization. Then, we report on a pilot clinical evaluation of the RiceWrist-S with one subject with incomplete SCI. The clinical evaluation methods are described in Section 3, including detailed description of performance metrics used for clinical and robotic assessment, while the results are reported in Section 3.2. Finally, we discuss the implications of the clinical study outcomes.

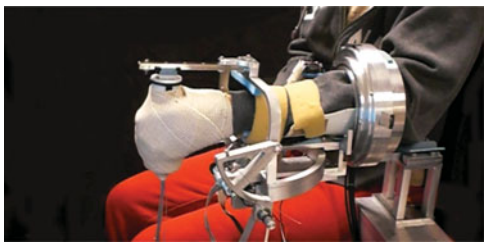

Fig. 1. (Colour online) RiceWrist-S – Forearm and wrist exoskeleton for rehabilitation, shown with participant with incomplete spinal cord injury.

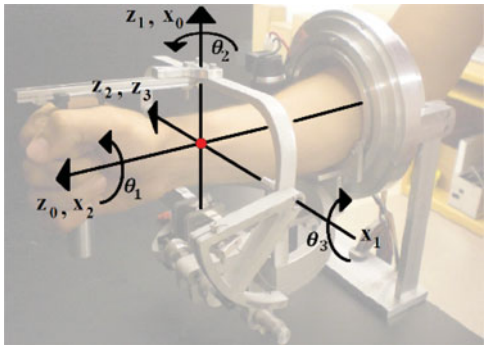

Fig. 2. (Colour online) Kinematic structure of RiceWrist-S, a 3-DOF serial RRR mechanism.

2. Device Description and Modelling

2.1. Design details

The RiceWrist-S is a purely rotational 3 DOF, electrically actuated forearm-wrist exoskeleton. The system employs a serial RRR manipulator and is capable of actuating the user's forearm (pronation/supination (PS)) and wrist (flexion/extension (FE) and radial/ulnar deviation (RU)) DOFs separately. The system also employs a passive DOF at the handle to add redundancy to the mechanism and correct for any misalignment that might occur due to the simplifying assumption that the three axes of wrist motion intersect at a point. In the neutral position (shown in Fig. 2), z_0, z_1 and z_2 coincide with the user's PS, FE and RU rotation axes respectively. Frame $\{1\}$ is coincident with frame $\{0\}$, then rotated $-\frac{\pi}{2}$ radians around x_0. The rotation θ_1 around z_0 corresponds to the user's PS rotation angle. Similarly, frame $\{2\}$ is coincident with frame $\{1\}$, then rotated $\frac{\pi}{2}$ radians around x_1. The rotation θ_2 around z_1 corresponds to the user's FE rotation angle. Frame $\{3\}$ is coincident with frame $\{2\}$, and the rotation around z_2 corresponds to the user's RU rotation angle. A more detailed evaluation of the kinematics of the device can be found in ref. [20].

In order to ensure zero backlash and low friction on the FE and RU joints, the RiceWrist-S uses cable drive transmissions, while the PS joint employs a frameless brushless motor in direct drive configuration. The cable transmission for the RU joint (Fig. 3 (a)) is achieved via a cable routing mechanism that allows remote placement of the actuator so as to minimise gravitational and inertial loading on the user. The primary benefit of the cable routing mechanism is that it enables placement of the RU joint actuator exactly below the FE rotation axis, decreasing the endpoint inertia of the device. Additionally, the cable routing mechanism enables achievement of a 1:24 transmission ratio with a compact design, providing high torque output and increasing the sensor resolution by a factor of 24. The motor power is transferred from the motor shaft to the transmission shaft via two steel cables, both of which are first fixed on the motor shaft and wound in opposite directions on the shaft, then wound around and fixed on the aluminum cylinders. The aluminum cylinders are threaded and coupled to the precision threaded steel transmission rod, allowing transmission of motor power to the transmission rod. To transfer power from the transmission rod to the device handle, one end of the transmission shaft is used as a capstan spool, and the capstan arc, coupled to the device handle, is driven by means of a cable drive system. The cables are pretensioned by screwing the aluminum cylinders in opposite directions, and two nuts are used to secure each cylinder and prevent cable

Table I. Sensor and actuator specifications for the RiceWrist-S upper limb rehabilitation robot.

Joint	**Actuator**	**Transmission**	**Sensor (Resolution)**
Forearm Pronation/Supination	Applimotion 165-A-18	Direct-Drive	MicroE Mercury-1500 (0.002°)
Wrist Flexion/Extension	Maxon RE-40 (148877)	Cable Drive (1:18)	Avago HEDS-5540 (0.01°)
Wrist Radial/Ulnar Dev.	Maxon RE-30 (310009)	Cable Drive (1:24)	Avago HEDS-5540 (0.0075°)

Table II. Achievable joint ranges of motion (ROM) and maximum continuous joint torque output values for RiceWrist-S. The required ROM and torque values for 19 (ADL) as extracted from[19] are also given for comparison.

	ADL		**RiceWrist-S**	
Joint	ROM (deg)	Torque (Nm)	ROM (deg)	Torque (Nm)
Forearm Pronation/Supination	150	0.06	180	1.69
Wrist Flexion/Extension	115	0.35	130	3.37
Wrist Radial/Ulnar Dev.	70	0.35	75	2.11

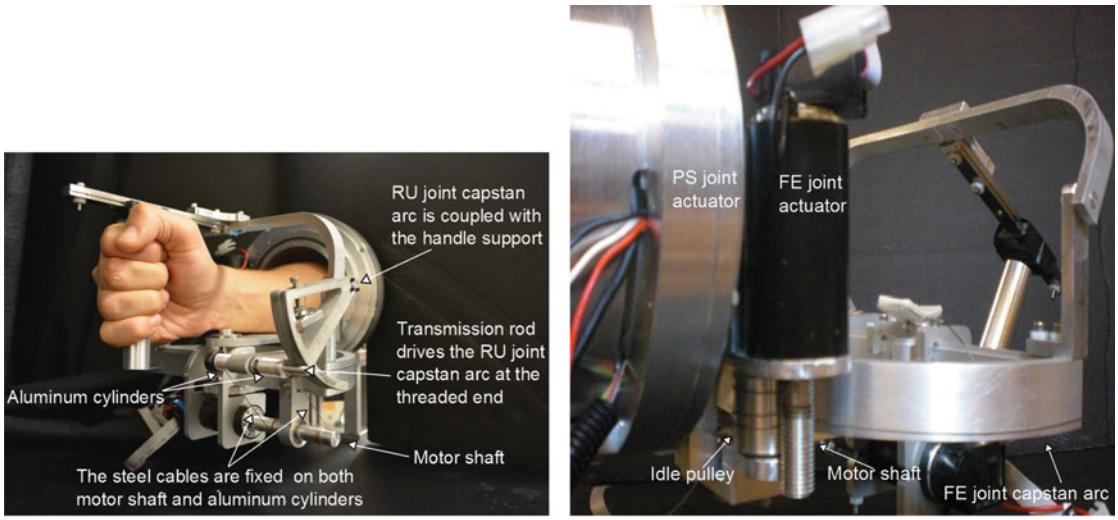

(a) (b)

Fig. 3. (Colour online) (a) Cable routing mechanism for the RU joint: power is transferred from the motor shaft to the transmission rod via a steel cable. The transmission rod drives the RU joint capstan arc, that is coupled with the handle support. (b) Cable routing mechanism for the FE joint: an idle pulley is employed to transfer actuation to the FE joint capstan arc, via a steel cable.

loosening. Actuation is provided by a Maxon RE-30 brushed DC motor with a CPT Avago 5540 HEDS optical encoder with 500 counts per revolution. The cable transmission for the FE joint is designed so that the distance of the FE actuator from the PS rotation axis is minimised, in order to keep the inertia of the device as low as possible. An idle pulley is employed to avoid collisions between the actuator and other device components (see Fig. 3 (b)). The transmission ratio for the FE joint is 1:18. We selected a Maxon RE-40 brushed DC motor with a CPT Avago 5540 HEDS optical encoder with 500 counts per revolution. The sensing resolution, actuator and transmission specifications, torque output, and ROM capabilities of the device are summarised in Tables I and II.

The safety of the subject is ensured via mechanical stops that are within the reachable range of motion for an unimpaired subject. Additionally, current saturation is applied in software to limit excessive torque command to the motors. Finally, multiple mechanical emergency stop buttons are employed which can be activated by the therapist at any time.

The RiceWrist-S also features a handle with an integrated force sensor, providing the ability to measure grip and interaction forces from the user during therapy. Our group was interested in

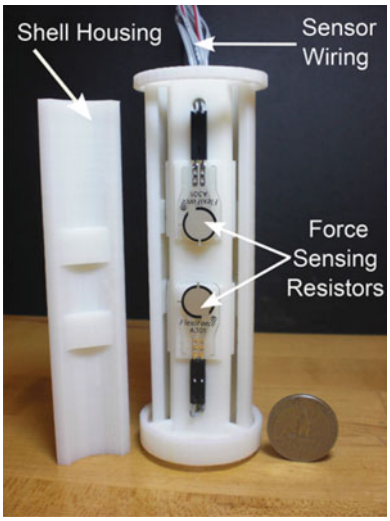

Fig. 4. (Colour online) The RiceWrist-Grip force sensing handle measures grip force via six FlexiForce A301 force sensing resistors.

incorporating a grip force sensor into the design since we have observed improved grip strength during therapy even though grip strength is not directly rehabilitated with our RiceWrist devices. The RiceWrist-Grip, shown in Fig. 4, can measure normal forces in three planes through six thin film force sensing resistors (FSRs). Force sensing resistors were employed for their moderate cost and form factor, the latter allowing easy incorporation into a cylindrical handle. The sensors are distributed in three pairs, with each pair of FSRs evenly spaced on the inner circumference of the handle. Three cylindrical shell slices, with two flats facing the sensors, are used so that all load is transferred to the FSRs. To control the load area on the FSRs, 1.5 mm thick and 8.5 mm diameter plastic cylinders were placed between the sensing area of the FSRs and the flats on the shells. The main body of the sensor and the shell slices were created by a 3D printing machine with 0.51 mm resolution from Acrylonitrile Butadiene Styrene (ABS) plastic. The RiceWrist-Grip weighs 92 g, is 34 mm in diameter, and 126 mm in length. The RiceWrist-Grip is easily incorporated into the RiceWrist-S, enabling real-time monitoring of grip strength during therapy.

2.2. Dynamical performance analysis

A critical design requirement for the RiceWrist-S is dynamic transparency which affects the ease of human-induced motion when the device is unpowered, since we rely on such an operation mode for assessment of subjects' movement quality. One way to characterise dynamic transparency is to quantify the inertial forces required to actuate the manipulator when the user is driving the robot. To do so, we calculated the generalised inertia ellipsoid (GIE) of the device for the complete joint-space. GIE, defined first in ref. [21], is a measure of required torque for a unit acceleration at a given configuration.

Let us define the generalised coordinates and the joint space dynamic model of the RiceWrist-S as

$$\boldsymbol{\theta} = [\theta_1\ \theta_2\ \theta_3]^T \tag{1}$$

$$\boldsymbol{\tau} = M(\theta)\ddot{\theta} + B(\dot{\theta}, \theta)\dot{\theta} + G(\theta) \tag{2}$$

where $\mathbf{M}$ is a 3×3 inertia matrix, $\mathbf{B}$ is a 3×3 matrix which represents Coriolis/centrifugal terms, $\mathbf{G}$ is the 3×1 gravity vector, and $\boldsymbol{\tau}$ is the 3×1 vector of the back-driving torque applied by the subject represented in the joint-space. We are interested in considering the inertial contribution of the torques required to back-drive the robot, hence let us assume $B(\dot{\theta}, \theta)\dot{\theta} = 0$, and neglect $\mathbf{G}$. As a result, (2) reduces to

$$\boldsymbol{\tau} = M(\theta)\ddot{\theta} \tag{3}$$

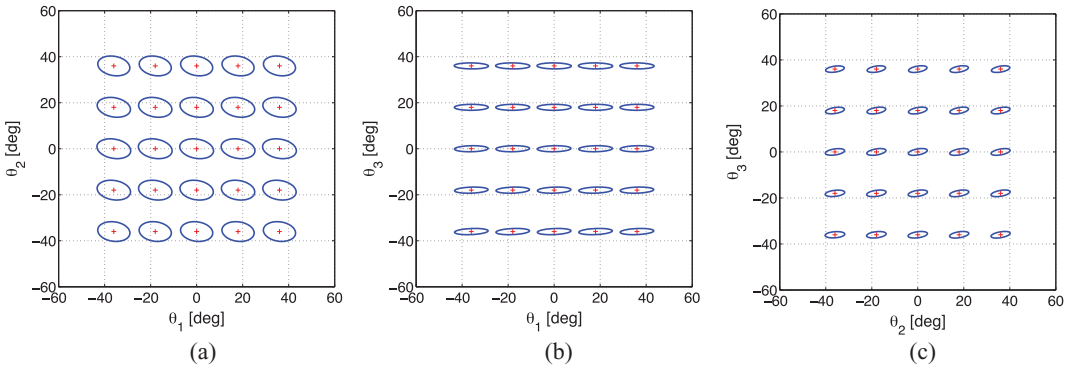

Fig. 5. (Colour online) Section views of the generalised inertia ellipsoid through the planes $\theta_3 = 0$ (a), $\theta_2 = 0$ (b), and $\theta_1 = 0$ (c), for different manipulator configurations.

Consider the constant unit joint accelerations, which describe the points on a spherical surface

$$\ddot{\theta}^T \ddot{\theta} = 1 \tag{4}$$

Combining (3) and (4), the torques required to obtain a unit acceleration can be computed by solving the following quadratic form:

$$\tau^T M^{-T}(\theta) M^{-1}(\theta) \tau = 1 \tag{5}$$

The analytical expression of the inertia matrix M as a function of generalised coordinates θ_1, θ_2 and θ_3 can be obtained using standard Lagrangian dynamical modeling methods,[22] and allows the definition of a quadratic form, as a function of only the generalised coordinates and inertial manipulator parameters: the generalised inertial ellipsoid (GIE).[21] Analysis of the GIE allows determination of the apparent resistance to motion perceived by the user when moving at constant acceleration, as a function of the direction of motion. The distance between a point on the surface of the ellipsoid drawn around the current manipulator kinematic status $\theta_c = (\theta_1, \theta_2, \theta_3)$ and the point θ_c itself gives a measure of the inertia perceived along the direction joining the point on the surface and θ_c. The generalised ellipsoid can be represented in a more synthetic and compact way by eigenvalue decomposition of the matrix $M^{-T}(\theta)M^{-1}(\theta)$. The eigenvectors of the matrix define the principal axes of the ellipsoid, while the reciprocals of the square of the eigenvalues define the semi-axes lengths. In the cases of the principal directions, the ellipsoid axes length gives an immediate measure of the necessary torque values to generate a unit joint acceleration along the corresponding principal direction.

For clarity of representation, section views of the GIE are reported in Fig. 5, obtained as a cut of the GIE through planes $\theta_3 = 0$, $\theta_2 = 0$, and $\theta_1 = 0$, respectively, for different manipulator configurations. The axes lengths vector $L_{|\theta_0}$ and the principal axes matrix $Dir_{|\theta_0}$ of the ellipsoid for the neutral position $\theta_0 = [\theta_1\ \theta_2\ \theta_3]^T$ are computed as

$$L_{|\theta_0} = [0.0185\ \ 0.0105\ \ 0.0033]^T \tag{6}$$

$$Dir_{|\theta_0} = \begin{bmatrix} 0.0367 & 0.1715 & 0.9845 \\ 0.0905 & 0.9805 & 0.1742 \\ 0.9952 & 0.0955 & 0.0205 \end{bmatrix} \tag{7}$$

The joint torque values at the neutral position computed using Equations 6 and 7 are given as

$$\tau_{|\theta_0} = [0.0201\ \ 0.0138\ \ 0.0047]^T Nm \tag{8}$$

In order to assess the configuration-dependence of the inertia perceived with respect to the device configuration, we initially evaluated the variability of principal directions, and assessed that they are mostly parallel to the cardinal axes of the manipulator (i.e. θ_1, θ_2 and θ_3). Since the principal direction orientation changes by less than $\pm$ 5 deg as a function of manipulator workspace, we

Table III. RiceWrist-S device characteristics.

	Static Friction	Inertia	Viscous Coeff.	CL Position Bandwidth
Joint	(N·m)	(kg·m^2)	($\frac{\text{Nm·s}}{\text{rad}}$)	(Hz)
Forearm Pronation/Supination	0.221	0.0258	0.428	3.5
Wrist Flexion/Extension	0.198	0.01165	0.085	6
Wrist Radial/Ulnar Deviation	0.211	0.0048	0.135	8.3

could analyze variability in intrinsic inertia by only evaluating the variability of GIE eigenvalues, throughout the manipulator's reachable workspace ($\pm$45 deg for all joints, 1031 evenly spaced points). The maximum variability is obtained for the PS joint, and approximately equals 10.8% of the value computed at the neutral position. The maximum variability of the other joints are 4% (FE) and 9% (RU), and demonstrates that variability in the eigenvalues of the inertial matrix is less than one order of magnitude compared to the values measured in the neutral position.

2.3. Device characteristics

In order to evaluate the potential of the RiceWrist-S for rehabilitation, we determined the resolution of the device using a similar approach presented in ref. [23], along with key device characteristics that affect dynamic performance. The end effector spatial resolution (ΔQ_E), is calculated by considering the Jacobian of the device ($J(\theta)$) and the joint space resolution vector (δ_θ), which includes the resolution values provided in Table I, for any configuration (θ) of the work space W as

$$\Delta Q_E = max\{\|J(\theta)\delta_\theta\|\}\forall\theta \in W \tag{9}$$

and was determined to be 2.1816×10^{-4} radians.

The mechanical characteristics of the device, including static friction, inertia, and viscous friction, are experimentally determined for every joint. The response of the system to a ramp position input is used to determine the static friction. The inertia and viscous friction are determined by investigating the response of the system to a step position command. While a more detailed description of these procedures can be found in ref. [20], the estimated parameters are reported in Table III for completeness. The closed loop position control bandwidth of the RiceWrist-S is identified by observing the device's ability to track a sine position input with a PD controller implemented for each individual DOF. We observed approximately 3.6 Hz, 6 Hz, and 8.3 Hz bandwidths for the PS, FE, and RU degrees-of-freedom, respectively.

Comparison between the experimentally-estimated joint inertia values shown in Table III and those obtained through dynamical modeling through (8) shows a strong quantitative agreement, with a maximum percentage error of 20% for the PS joint, that accounts for an error in the estimated inertia of only $6{\cdot}10^{-3}$ kg·m^2. The model also correctly predicts that the joint with the highest reflected inertia is the PS joint, whose value of intrinsic inertia is 1.5 times higher than that of the FE joint. Finally, the joint with the least inertia is the RU joint, that is approximately aligned with the axes corresponding to the lower eigenvalue of the inertia matrix, with an inertia approximately one third of that of FE joint.

2.4. Grip force sensor calibration

The RiceWrist-Grip force sensing handle incorporates force sensing resistors as a cost-effective means of measuring grip strength. The Tekscan FlexiForce A301 force sensing resistor was chosen due to its size (25.4 mm long 0.203 mm thick), 3% linearity, 0-440 N force range, and 5 μs response time. The resistance of the A301 FSR changes inversely with force, so utilizing an inverting op-amp circuit gives a linear relationship between force and voltage:

$$V = -V_{in}\frac{R_f}{R_{FSR}(F)} \tag{10}$$

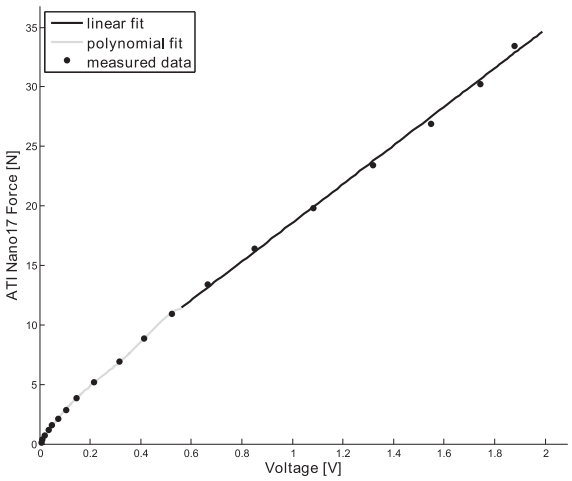

Fig. 6. Calibration of a single FSR with using the ATI Nano17 force sensor. For low forces (< 11.5 N), a polynomial fitting was used, while a linear fit was used for after this break in region.

where V is the FSR output voltage, V_{in} the input voltage to the FSR, R_f a feedback resistor, and $R_{FSR}(F)$ is the variable resistance from the FSR, which is a function of the applied force F. The feedback resistor and input voltage to the FSR need to be chosen appropriately to allow for the output voltage to remain within the op-amp supply voltage range for every admissible value of applied force. For our purposes, R_f was chosen to be 100 kΩ and V_{in} was chosen to be -4.5 V, since forces under 100 N were expected on a single force sensing resistor. To calibrate the sensors, an ATI Industrial Automation Nano17 SI-25-0.25 six-axis force/torque transducer with 0.00625 N resolution was used. A single FSR was prepared for calibration by placing a plastic cylinder between the FSR and the Nano17 force sensor and applying manual compression forces to the FSR. The resulting calibration (see Fig. 6) shows that at low forces (< 11.5 N), the sensor had a nonlinear output appropriately described with a polynomial fitting (such as that used in ref. [24]), while for larger forces there existed a linear relationship. The coefficient of determination (R^2) in the linear portion of Fig. 6 was 0.9964, verifying the existence of a linear correlation between the two variables in this region. The ATI Nano17 is limited to 35 N in the z-axis so calibration was only performed up to 35 N. It should be noted that the voltage of the FSR could approach 6 V (limited by the op-amp) and so forces of up to 100 N could be measured. The linearity of the FSRs for voltages above the range shown in Fig. 6 has been previously confirmed experimentally with an Instron machine (up to 6 V and 175 N), justifying the extrapolation.

3. Clinical Case Study

In order to validate the use of the RiceWrist-S with the RiceWrist-Grip force sensing handle for clinical use in upper extremity rehabilitation, we conducted a case study with an individual with chronic incomplete spinal cord injury. In the following sections, we describe the methods and results of this pilot evaluation. We hypothesised that with this novel device the robot-aided therapy would result in observable gains in clinical measures of motor impairment, and in improvements in movement smoothness, as we have observed in previous studies of robotic rehabilitation.[25]

3.1. Methods

A 45-year-old male, right handed, with incomplete SCI at the C3-5 level, classified as American Spinal Injury Impairment Scale (AIS) C and 83 months post-injury, participated in ten sessions of robotic-assisted arm training over 20 days of training, approximately four times per week, subject to a protocol approved by all participating institutions. The participant was highly active and independent in his powered wheelchair. Motor impairment in the distal component of his upper limb, including voluntary opening/closing of the hand or isolated finger movements, was greater when compared to

the proximal components of the extremity, such as wrist and forearm movements. During the course of training, he did not participate in any other intensive occupational therapy program.

Set-up of the system and donning of the exoskeleton took approximately ten minutes. The subject was seated on a chair with his left arm placed inside the RiceWrist-S exoskeleton, and fixed to the device through Velcro and straps for minimizing the relative motion between the forearm and the device. Each session began by defining the subject's active range of motion, for each DOF (calibration session). After calibration, an evaluation session was conducted where the subject was asked to perform visually-guided target hitting movements when back-driving the unpowered device through one of its DOFs. Later, a training session was administered, that involved the same target-hitting tasks, but with the robot commanded to display a resisting force field proportional to the movement velocity at the intended joint, while all other joints of the device were kept stationary via control. The level of resistance was changed from session to session by the therapist according to the observed performance of the subject. The therapist aimed to increase resistance and thereby the challenge and engagement of the subject, but also was observant of the subject's fatigue level when choosing resistance levels. After completion of the evaluation and therapy for the first DOF, the process was repeated for the other DOFs. All training sessions were conducted by a physical therapist (N.Y.) who had previous experience with robotic-assisted training and rehabilitation of adults with incomplete spinal cord injury.

3.1.1. Clinical assessment measures. The efficacy of the robotic rehabilitation protocol was evaluated using recognised clinical assessment techniques. Specifically, we tested upper extremity muscle strength, motor performance function, grip and pinch forces before training and immediately after the ten sessions of training. The strength of selected upper extremity key muscles (elbow flexors, wrist extensors, elbow extensors, finger flexors, and finger abductors) was scored according to American Spinal Injury Association (ASIA) guidelines between 0 and 5 (total score, range 0-25).[26]

Arm and hand function performance were measured with both the Jebsen-Taylor Hand Function Test (JTHFT) and Action Research Arm Test (ARAT).[27,28] The JTHFT is a standardised 7-item test designed to evaluate various hand functions that resemble daily life activities, including writing, simulated page turning, picking up small common objects, stacking checkers, simulated feeding, lifting large and light objects, and lifting large and heavy objects. The sentence writing task was not included in the score due to severe hand dysfunction on the non-dominant side for our participant. Time of performance is recorded for each task. JTHFT has been used widely to measure upper extremity motor function in stroke and SCI[29] and has an established validity,[30] reliability,[31] and capacity for detecting changes in performance.[32,33] The Action Research Arm Test (ARAT) is a standardised test of unilateral hand and upper limb function that consists of 19 items divided into four sub-tests including grasp, grip, pinch and gross movement.[28] Although the ARAT was originally designed to measure arm and hand functions after stroke,[32,34,35] it has been successfully used in SCI.[36,37] All tasks are scored on a 4 point ordinal scale ranging from 0-3 where 0 = no movement; 1 = performs test partially; 2 = complete test, but takes abnormally long or has great difficulty; and 3 = normal movement, giving a possible range of 0-57.

In addition to these measures of arm and hand function, grip strength data were collected before and after each training session. Manual grip strength was measured with a hand-held standard adjustable dynamometer (Lafayette Instrument, Model 78010) in the sitting position with shoulder adducted, elbow flexed and forearm in mid-position. The subject was asked to perform three maximal voluntary contractions, and the maximum value of each attempt was recorded.[38] Following the assessment with the dynamometer, the same testing procedure was repeated for the instrumented grip force measurement device. A pinch gauge was used to measure maximum pinch force, which was averaged over attempts with each hand. A minimum possible value of 0 kgf was assigned when the participant could not actively squeeze the pinch meter between the thumb and index finger.[39] Finally, the subject was asked to rate his fatigue and discomfort/soreness level on a visual analogue scale ranging from 0-100, before and after each training session.

3.1.2. Robotic data assessment measures. Motion data recorded during the evaluation portion of each therapy session were quantitatively analysed in order to evaluate if improvement in the quality of upper extremity goal-directed movements could be detected. Movements were initially segmented into individual point-to-point movements. This was done by selecting a threshold α of the peak velocity v_{max}, measured during each movement, which was then used to define both the instant of

movement start t_{in} and of movement end t_{fin}. These points in time represent the first and last instance in which the condition $|v(t)| > \alpha|v(t_{max})|$ is verified within a movement, where t_{max} is the time at which maximum velocity occurs. For the purposes of this analysis, α has been set to 0.05. Although there is no general consensus for the hypothesis that wrist pointing movements have symmetric velocity profiles, and preliminary studies are actually in support of their moderate asymmetry,[40] this segmentation algorithm has been selected because it is standard in the robotics and motor control literature,[41] and allows a direct comparison of our results with those deriving from other protocols and systems. Due to the inherent unidimensionality of the task (the maximum straight line deviation of successful movements was less than 0.5 deg), velocity profiles and subsequent derivatives were calculated as time derivatives of the measured joint angles. Encoder data were acquired continuously at 100 Hz; velocity profiles and higher-order derivatives were extracted in post-processing using a Savitzky-Golay filter, which has been purposively conceived to be optimal in minimizing amplified noise through differentiation, performing a local fourth order polynomial fit in a moving window of amplitude 100 ms (i.e. containing 10 samples).

Two indices of performance were calculated for each point-to-point movement, in order to verify the hypothesis that smoothness of movement would be increased by robot-aided therapy. The considered indices of performance were the Movement-Arrest-Period-Ratio (MAPR)[42] and a normalised measure of the sum-of-jerk of the measured profile (NSOJ), similar to the one used in ref. [43].

The MAPR is a simple and robust method for assessing movement smoothness that quantifies the departure of the measured velocity profile from a single peaked, approximately bell-shaped profile, considered the "reference" movement profile for healthy point-to-point movements of the upper arm.[41,44,45] The MAPR is defined as the percentage of the total movement duration in which the measured velocity is higher than a threshold of v_{max}, as:

$$MAPR = \frac{T_1}{t_{end} - t_{in}}, \tag{11}$$

where T_1 is defined as the total time in which the condition $v(t) > \beta v_{max}$ is verified and can be expressed as the integral of a boolean time-series, as:

$$T_1 = \int_{t_1}^{t_{end}} (v(t) > \beta v_{max}) \mathrm{d}t \tag{12}$$

For the purposes on analysis in this study, the threshold β was set to 0.25.

Sum-of-jerk (SOJ) metrics have been widely employed to quantify the smoothness of movements of subjects undergoing robot-aided therapy, mostly in the literature of post-stroke robot-aided rehabilitation. Computation of SOJ metrics requires differentiated encoder signals, and therefore implies applicability only to robotic systems with high resolution joint angle measurement.[43,46,47] We consider that the mechanical structure and the sensing subsystem of the RiceWrist-S has a high accuracy in measuring the end-effector position, so that the measured profiles during pointing movements are minimally affected by quantization. In this paper, a specific form of normalised SOJ (NSOJ) measure was considered, since it has been shown to be strictly increasing with the amount of onset time between submovements,[43] and because normalization makes the calculated index insensitive to changes in movement duration.[47] The specific form used for the NSOJ metrics is obtained by normalizing the sum-of-jerk by the cube of mean velocity, as:

$$NSOJ = -\frac{1}{v_{mean}^3 (t_{end} - t_{in})} \int_{t_{in}}^{t_{fin}} |\dddot{\theta}(t)| \mathrm{d}t, \tag{13}$$

where the minus sign is introduced so that NSOJ defines a measure of trajectory smoothness, and not of its inverse.

It should be noted that the fact that observed velocity profiles are asymmetric is in contrast with the minimum jerk hypothesis and thus would suggest that criteria such as NSOJ may not accurately measure deviation from the ideal profiles. However, despite the reduction in accuracy, the degree of mismatch between the minimum jerk trajectory and the average movement extracted during our experiments with healthy subjects is fairly small,[40] compared to the highly non-bell shaped movements

Table IV. Functional scores before and after robotic therapy.

Test	Baseline	Post-treatment
ASIA UEMS	15	15
JTHFT (seconds)	99.1	93.8
Flipping cards	15	15.2
Picking up small objects	27	28.3
Simulated feeding	12.4	11.7
Lifting big objects (light)	12.3	13
Lifting big objects (heavy)	20.8	14.6
ARAT (0-57)	29	31
Grasp (0-18)	12	12
Grip (0-12)	7	7
Pinch (0-18)	4	6
Gross Movement (0-9)	6	6
Pinch Force (kgf)	3	2.8
Grip Force (kgf)	11	14

extracted during therapy with SCI subjects, thus enabling the use of minimum jerk-based measures for heavily impaired subjects.

For each evaluation session, the values of MAPR and NSOJ were calculated for the 20 point-to-point movements performed, separately for each degree of freedom. The values corresponding to the first and last evaluation session of the robotic therapy program were considered for statistical inference (three tests for each movement direction (FE, RU, PS), giving dof = 19, and a single test including the combination of movements in all directions, all dof = 59) using the non-parametric Wilcoxon signed rank test,[48] in order to test the null hypothesis, for which the indices of smoothness calculated during the two sessions come from a distribution with the same median.

3.2. Case study results

3.2.1. Clinical assessment. Table IV reports the values obtained through the clinical assessment tests. The results show improvements in the JTHFT as indicated by decreases in the amount of time necessary to execute functional tasks. Improvements in ARAT attributed to pinch, and increases in grip strength were found. However, the overall improvement in ARAT is lower than the minimal clinically meaningful change (5.7 points).[49] Performance for the other clinical assessments stayed constant from pre- to post-treatment. For example, at the conclusion of therapy, the subject's manual muscle test score did not show any change; however, a 1 point increase was observed in finger flexors (flexor digitorum profundus, middle finger, level of spinal innervation = C8). Manual grip strength improved from 11 kgf to 14 kgf, which possibly translated into improvement of lifting heavy objects in JTHFT - from a total 21 sec to 15 sec, the time necessary to grasp, lift and release five weighted cans (0.45 kg/can). The only positive change that occurred in ARAT was in the pinch subgroup, particularly seen in holding a spherical marble between the thumb and middle finger and between the thumb and index finger (from a score of 2 to 3).

The pinch strength assessment requires the subject to pinch a gauge between the thumb and index finger in order to measure isolated pinch forces, while the ARAT pinch subtest consists of tasks which rely on dexterous manipulation and positioning of the fingers, a more dynamic task. We hypothesise that over the course of the robotic therapy, the subject has improved overall in upper limb function, and therefore manipulating and moving small objects shows greater gains than direct measurement of pinch strength, though both assessments are focused on pinch capabilities of the subject.

The subject's self-report on fatigue and discomfort/soreness varied after each session, compared to before training. For example, for five of the ten sessions he reported an increase in fatigue level (average 36 points), though at other times he reported no change (after one session) or a decrease (after four sessions) in fatigue level (average -14 points). A similar pattern of variability was observed for discomfort/soreness level. For two sessions he reported a decrease in discomfort/soreness (average 23 points), while for eight sessions he reported an increase in discomfort/soreness level (average 17 points). All symptoms were localised to left arm/shoulder and upper back, and did not last longer than

Table V. Analysis of movement smoothness during the evaluation sessions.

	MAPR					**NSOJ**				
	Pre		**Post**		**Pre vs. Post**	**Pre**		**Post**		**Pre vs. Post**
Measure/DOF	Mean	Std	Mean	Std	*p* value	Mean	Std	Mean	Std	*p* value
FE	0.503	0.159	0.616	0.126	**0.0215**	−0.0131	0.0136	−0.0047	0.0027	0.068
RU	0.525	0.180	0.598	0.165	0.172	−0.0083	0.005	−0.022	0.0143	$6.2{\cdot}10^{-4}$
PS	0.520	0.238	0.605	0.151	0.324	−0.0313	0.0331	−0.0071	0.006	$\mathbf{3.0 \cdot 10^{-6}}$
All	0.516	0.192	0.607	0.146	**0.0084**	−0.0176	0.023	−0.011	0.012	**0.026**

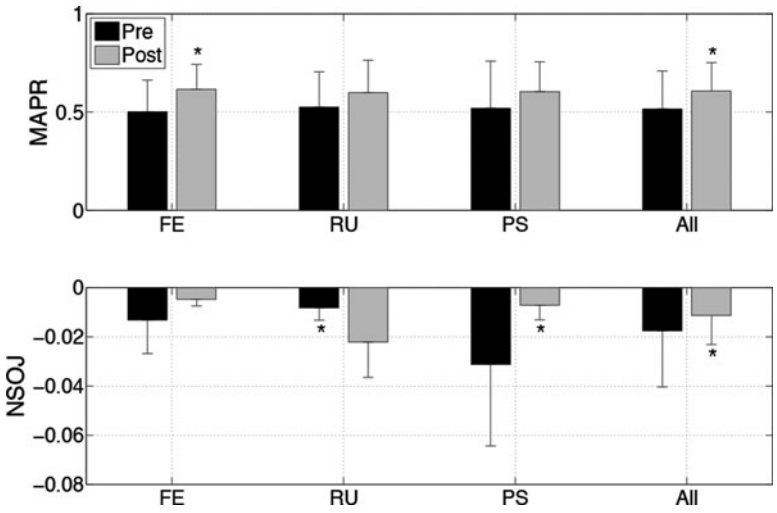

Fig. 7. Bar plot with error bars describing the two measures of smoothness computed during the first (Pre) and last (Post) session of therapy, representing mean and standard deviation of the twenty movements for every degree of freedom conducted during the assessment. An asterisk in proximity of the bar to the right/left indicates rejection of the null hypothesis at the 0.05 significance level, with the bar on the right/left having a higher mean (increased smoothness).

24 hours. Therefore, none of the training sessions were cancelled due to excessive discomfort/soreness or fatigue.

3.2.2. Robotic data assessment. The analysis of robotic data measured during evaluation sessions supports the hypothesis that robot-aided training increased smoothness of the participant's movements. Specifically, MAPR measures increased for movements in each degree of freedom. Pre-post comparison provided strong statistical significance for increased MAPR for FE movements and for the combination of all degrees of freedom, but not for RU and PS movements alone. However, the mean MAPR value for both RU and PS increased at the end of therapy, compared with the measurement in the first session. NSOJ shows a less consistent trend, for which smoothness increased with therapy for FE and PS movements, but not for RU movements. Pre-post comparison provides statistical significance of increased smoothness for PS movements and for the combination of all movements, weak significance for FE movements ($p = 0.068$) but strong significance for a decrease in movement smoothness for RU movements. This might be influenced by a fatigue effect given by the fact that during all sessions, the evaluation session for RU movements was administered last in the protocol, i.e. after evaluation and therapy sessions for both FE and PS. The indices of smoothness calculated and the results of the statistical analysis are reported in Fig. 7 and Table V.

3.2.3. Grip force assessment. Grip strength of the subject was obtained for each of the ten treatment sessions both pre- and post-therapy. Grip strength was recorded first for three trials using the RiceWrist-Grip followed by three trials with a hand dynamometer (Model 78010 Lafayette Hand Dynamometer). For all cases, the subject was instructed to exert maximum grip effort for approximately two seconds with 10–20 seconds of rest in between maximum grip efforts. The

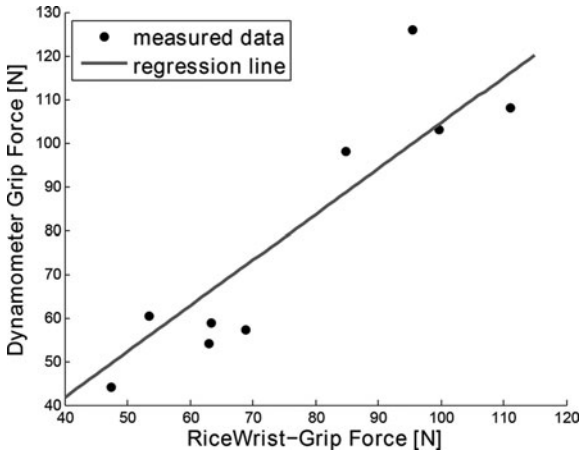

Fig. 8. Comparison of post-treatment grip forces across sessions 2-10, measured by the RiceWrist-Grip and Lafayette hand dynamometer.

participant had a few minutes to rest between using each device. Grip force from the dynamometer was recorded visually with a resolution of 4.9 N. Hand dynamometer grip force was taken as the average of the three trials. For the grip force sensor, grip force was calculated by first converting the voltage readings from the FSRs to force through the calibration in Fig. 6. To calculate total grip force, we considered the measured forces as pressures on the circumference of the handle, similar to,[50] and calculated total grip force as:

$$F_{grip} = \frac{1}{n}\sum_{i=1}^{n} F_i \tag{14}$$

where F_i are the equivalent forces on the circumference of the handle, F_{grip} is the grip force, and n is the number of forces on the handle, which for our case is $n = 3$. Each component of the grip force is computed by summing the values of the forces on the corresponding vertical pairs of FSRs. Grip force was averaged across the extent of the trial ($\sim$ 2 s). Then, the three average values for each trial were averaged to obtain the mean grip strength.

We report mean grip force measurements post-treatment for Sessions 2 through 10 for the participant's left hand (Session 1 was excluded due to incomplete data collection), and compare this estimate of grip force with that obtained through the commercial dynamometer. Results for the mean grip force measurements from the RiceWrist-Grip and hand dynamometer are shown in Fig. 8. The resulting correlation coefficient ($R^2 = 0.8335$) shows that there is good correlation between the two methods of grip force assessment, thereby providing preliminary validation of the use of the RiceWrist-Grip for assessment of grip force capabilities of subjects.

4. Discussion and Conclusions

We present the novel design and pilot clinical study validation of the RiceWrist-S, a custom-developed wrist exoskeleton for incomplete spinal cord injury robot-aided therapy. The kinematic structure of the RiceWrist-S is chosen so that every actuated degree of freedom directly corresponds to an individual human anatomic rotation. By incorporating a custom cable drive transmission that minimises inertial and gravitational loading on the proximal joints, we realise an increase in the dynamic transparency of the exoskeleton when it is in unpowered mode. The reduction of inertia is demonstrated through the analysis of the GIE through the three-dimensional workspace of the manipulator. The GIE analysis shows that the RiceWrist-S has configuration-independent intrinsic dynamical properties throughout the workspace, with a maximum ratio between highest inertia to lowest inertia across actuated joints equal to 5, similar to state-of-the-art systems such as the one presented in refs. [17, 51]. However, the presented device does not require high-accuracy mechanical parts and expensive transmission components as the differential gear used in ref. [17]. Moreover, the use of cable drive transmission contributes to the low friction characteristic of the RiceWrist-S. The maximum static friction values

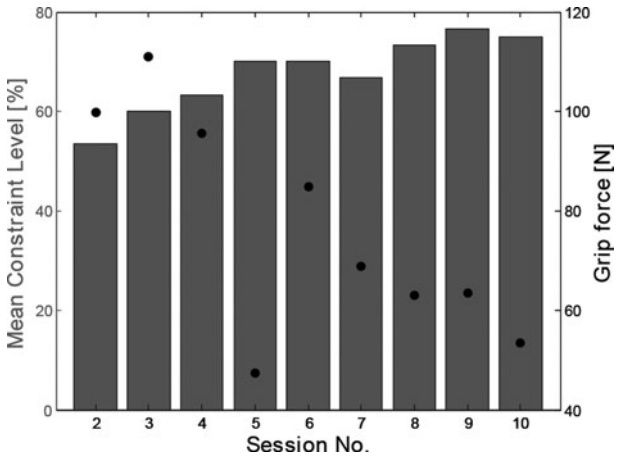

Fig. 9. Post-treatment grip force measurements and mean constraint level during training portion of therapy across sessions 2-10.

are smaller than 13%, 6%, and 10% of the continuous torque at PS, FE, and RU joints, with a maximum value of 0.22 Nm of static friction. Additionally, the kinematic structure reduces the measurement of the hand orientation and control of the device to joint space tasks, removing the need for inverse or forward kinematics calculations.

In order to further validate our RiceWrist-S and grip force sensor as clinically appropriate, we conducted a single case study with one participant presenting with chronic incomplete spinal cord injury at the cervical level. Results from this pilot trial are significant in demonstrating that repetitive training of certain movements with the RiceWrist-S are feasible in rehabilitation of upper extremity motor functions in incomplete SCI. The clinical findings reinforce results from our prior pilot trial that repetitive training of arm and wrist movements (with MAHI Exo-II) in incomplete SCI can be associated with motor gains in hand movements.[10,52] More specifically, the repetitive training of forearm and wrist muscles with the RiceWrist-S device has shown mild increase in hand grip and selective hand functions such as pinch grip and lifting heavy objects. Two smoothness of movement metrics have been used to assess the efficacy of the robotic training protocol by using the acquired robotic data during evaluation sessions where the participant backdrives the robot. In comparisons of pre- and post-training robotic measures, the subject showed improvement in terms of both MAPR, the percentage of the total movement duration in which the measured velocity is higher than a threshold of maximum velocity, and NSOJ, a normalization of the sum of-jerk by the cube of mean velocity.

The RiceWrist-S incorporates a grip force sensor whose design was validated by the moderate to strong correlation between the RiceWrist-Grip force measurements and those acquired with a hand dynamometer at the conclusion of each therapy session. A correlation of $R^2 = 0.8335$ between the hand dynamometer and RiceWrist-Grip for post-session measurements was found. Although the relationship was not fully linear, discrepancies could result from fatigue of the subject, since our protocol always required measurement from the grip sensor first or by reduced resolution in the visual readings of dynamometer data. However, by using the RiceWrist-Grip, measurements can also be obtained during continuous operation of the robot, in real-time. An additional result of interest was the relation between values of grip strength post therapy for varying constraint levels during therapy. A moderate negative linear correlation was observed between the value of grip force measured after therapy and the mean constraint level for that session ($R^2 = 0.6437$, with a significant negative slope at the chosen significance level $p < 0.05$). This relationship can be seen in Fig. 9, where the mean constraint level is represented as bars, and the grip force is represented by dots. These trends suggest that constraint-level induced fatigue is responsible for the decrease in measured grip force, especially when the mean constraint level is increased. However, no significant correlation was found between the same measure (post-session grip force) and the self-assessed fatigue test that was administered after each session. Moreover, no significant correlation was found between mean constraint level and self-assessed fatigue. This discrepancy may be attributable to the subjective scale used for fatigue testing. In contrast to these findings with the RiceWrist-Grip, the clinical assessment of grip strength as measured with the dynamometer took place two days after completion of the final

robot-aided therapy session, and showed a 3 kgf (27%) increase in grip strength. It is likely that the evaluation sessions that were coincident with therapy sessions may reflect increased levels of fatigue, as demonstrated by the reduction in grip force as measured by the RiceWrist-Grip.

The promising results of this study suggest further exploration of the therapeutic effect of training with the RiceWrist-S exoskeleton for subjects with incomplete SCI, assessed using objective robotic measures of motor impairment. The RiceWrist-Grip data collected during therapy suggest the need for more fine-tuned or even real-time monitoring of the fatigue levels of participants. Further, these measurements could be included in assist-as-needed protocols, in order to select the appropriate challenge level that would allow optimal therapeutic outcomes.

Acknowledgements

This work was supported in part by grants from Mission Connect, a project of the TIRR Foundation, the National Science Foundation Graduate Research Fellowship Program under Grant No. 0940902, NSF CNS-1135916, and H133P0800007-NIDRR-ARRT

References

1. J. D. Schaechter, "Motor rehabilitation and brain plasticity after hemiparetic stroke," *Prog. Neurobiology* **73**, 61–72 (Jun. 2004).
2. N. Hogan, H. I. Krebs, B. Rohrer, J. J. Palazzolo, L. Dipietro, S. E. Fasoli, J. Stein, R. Hughs, W. R. Frontera, D. Lynch and B. T. Volpe, "Motions or muscles? Some behavioral factors underlying robotic assistance of motor recovery," *J. Rehabil. Res. Dev.* **43**(5), 605 (2006).
3. V. R. Edgerton, N. J. K. Tillakaratne, A. J. Bigbee, R. D. de Leon and R. R. Roy, "Plasticity of the spinal neural circuitry after injury," *Annu. Rev. Neurosci.* **27**(1), 145–167 (Jul. 2004).
4. J. V. Lynskey, A. Belanger and R. Jung, "Activity-dependent plasticity in spinal cord injury," *J. Rehabil. Res. Dev.* **45**(2), 229–240 (Dec. 2008).
5. A. Go, D. Mozaffarian, V. Roger, E. Benjamin, J. Berry, W. Borden, D. Bravata, S. Dai, E. Ford, *et al.*, "Heart disease and stroke statistics–2013 update: A report from the American Heart Association," *Circulation* **127**, e8 (2013).
6. Anon, "Spinal Cord Injury Facts and Figures at a Glance," *National Spinal Cord Injury Statistical Center* (Feb. 2012).
7. M. Berkowitz, *Spinal Cord Injury: An Analysis of Medical and Social Costs* (Demos Medical Pub, 1998).
8. A. Lo, P. Guarino, L. Richards, J. Haselkorn, G. Wittenberg, D. Federman, R. Ringer, T. Wagner, H. Krebs, B. Volpe *et al.*, "Robot-assisted therapy for long-term upper-limb impairment after stroke," *New England J. Med.* **362**(19), 1772–1783 (2010).
9. C. Bütefisch, H. Hummelsheim, P. Denzler, and K. Mauritz, "Repetitive training of isolated movements improves the outcome of motor rehabilitation of the centrally paretic hand," *J. Neurological Sci.* **130**(1), 59–68 (1995).
10. N. Yozbatiran, J. Berliner, M. K. O'Malley, A. U. Pehlivan, Z. Kadivar, C. Boake and G. E. Francisco, "Robotic training and clinical assessment of upper extremity movements after spinal cord injury: a single case report," *J. Rehabil. Med.* **44**(2), 186–188 (2012).
11. H. I. Krebs, J. J. Palazzolo, L. Dipietro, M. Ferraro, J. Krol, K. Rannekleiv, B. T. Volpe and N. Hogan, "Rehabilitation robotics: Performance-based progressive robot-assisted therapy," *Auton. Robots* **15**, 7–20 (Jun. 2003).
12. E. Wolbrecht, V. Chan, D. Reinkensmeyer and J. Bobrow, "Optimizing compliant, model-based robotic assistance to promote neurorehabilitation," *IEEE Trans. Neural Syst. Rehabil. Eng.* **16**(3), 286–297 (2008).
13. S. E. Fasoli, H. I. Krebs, J. Stein, W. R. Frontera and N. Hogan, "Effects of robotic therapy on motor impairment and recovery in chronic stroke," *Arch. Phys. Med. Rehabil.* **84**(4), 477–482 (2003).
14. R. Colombo, F. Pisano, S. Micera, A. Mazzone, C. Delconte, M. C. Carrozza, P. Dario and G. Minuco, "Robotic techniques for upper limb evaluation and rehabilitation of stroke patients," *IEEE Trans. Neural Syst. Rehabil. Eng.* **13**(3), 311–324 (2005).
15. S. Hesse, G. Schulte-Tigges, M. Konrad, A. Bardeleben and C. Werner, "Robot-assisted arm trainer for the passive and active practice of bilateral forearm and wrist movements in hemiparetic subjects." *Arch. Phys. Med. Rehabil.* **84**(6), 915–20 (2003).
16. J. Oblak, I. Cikajlo and Z. Matjacic, "Universal haptic drive: A robot for arm and wrist rehabilitation," *IEEE Trans. Neural Syst. Rehabil. Eng.* **18**(3), 293–302 (2010).
17. H. I. Krebs, B. T. Volpe, D. Williams, J. Celestino, S. K. Charles, D. Lynch and N. Hogan, "Robot-aided neurorehabilitation: A robot for wrist rehabilitation," *IEEE Trans. Neural Syst. Rehabil. Eng.* **15**(3), 327–335 (2007).
18. V. Squeri, L. Masia, P. Giannoni, G. Sandini and P. Morasso, "Wrist rehabilitation in chronic stroke patients by means of adaptive, progressive robot aided therapy," *IEEE Trans. Neural Syst. Rehab. Eng.*, **22**(2), 1–14, (2013).

19. J. C. Perry, J. Rosen and S. Burns, "Upper-limb powered exoskeleton design," *IEEE/ASME Trans. Mechatronics* **12**(4), 408–417 (2007).
20. A. U. Pehlivan, C. Rose and M. K. O'Malley, "System characterization of ricewrist-s: A forearm-wrist exoskeleton for upper extremity rehabilitation," in *Proceedings of the 2013 IEEE International Conference on Rehabilitation Robotics (ICORR).* IEEE (2013) pp. 1–6.
21. H. Asada, "A geometrical representation of manipulator dynamics and its application to arm design," *J. Dyn. Syst. Meas. Control* **105**(3), 131–142 (1983).
22. L. Sciavicco and L. Villani, *Robotics: Modelling, Planning and Control* (Springer, 2009).
23. R. Brewer, A. Leeper, and J. K. Salisbury, "A friction differential and cable transmission design for a 3-dof haptic device with spherical kinematics," *Proceedings of the 2011 IEEE/RSJ International Conference on Intelligent Robots and Systems (IROS),* IEEE (2011) pp. 2570–2577.
24. M. Ferre, I. Galiana and R. Aracil, "Design of a lightweight, cost effective thimble-like sensor for haptic applications based on contact force sensors," *Sensors* **11**, 11 495–509 (Jan. 2011).
25. O. Celik, M. K. O'Malley, C. Boake, H. S. Levin, N. Yozbatiran and T. A. Reistetter, "Normalized movement quality measures for therapeutic robots strongly correlate with clinical motor impairment measures," *IEEE Trans. Neural Syst. Rehabil. Eng.* **18**(4), 433–444 (2010).
26. F. Maynard Jr. and M. Bracken, "Creasey," G, Ditunno. JF, Donovan. WH, Ducker. TB, Garber. SL, Marino RJ, Stover SL, Tator CH, Waters RL, Wilberger, JE, Young WSO "International Standards for Neurological and Functional Classification of Spinal Cord Injury, Americam Spinal Injury Association." Spinal Cord, **35**(5), 266–74 (1997).
27. R. Jebsen, N. Taylor, R. Trieschmann, M. Trotter and L. Howard, "An objective and standardized test of hand function." *Arch. Phys. Med. Rehabil.* **50**(6), 311–319 (1969).
28. R. C. Lyle, "A performance test for assessment of upper limb function in physical rehabilitation treatment and research," *Int. J. Rehabil. Res.* **4**(4), 483–492 (1981).
29. R. Martin, K. Johnston and C. Sadowsky, "Neuromuscular electrical stimulation–assisted grasp training and restoration of function in the tetraplegic hand: A case series," *Am. J. Occup. Ther.* **66**(4), 471–477 (2012).
30. E. Davis Sears and K. C. Chung, "Validity and responsiveness of the jebsen–taylor hand function test," *J. Hand Surg.* **35**(1), 30–37 (2010).
31. M. E. Hackel, G. A. Wolfe, S. M. Bang and J. S. Canfield, "Changes in hand function in the aging adult as determined by the jebsen test of hand function," *Phys. Ther.* **72**(5), 373–377 (1992).
32. J. A. Beebe and C. E. Lang, "Relationships and responsiveness of six upper extremity function tests during the first 6 months of recovery after stroke," *J. Neurologic Phys. Ther. (JNPT)* **33**(2), 96 (2009).
33. T. T. Francis and P. Reddappa, "Comparative study on the wrist positions during raise maneuver and their effect on hand function in individuals with paraplegia," *Top. Spinal Cord Injury Rehabil.* **19**(1), 42–46 (2013).
34. J. H. van der Lee, V. de Groot, H. Beckerman, R. C. Wagenaar, G. J. Lankhorst and L. M. Bouter, "The intra- and interrater reliability of the Action Research Arm test: A practical test of upper extremity function in patients with stroke," *Arch. Phys. Med. Rehabil.* **82**(1), 14–19 (2001).
35. C. E. Lang, D. F. Edwards, R. L. Birkenmeier and A. W. Dromerick, "Estimating minimal clinically important differences of upper-extremity measures early after stroke," *Arch. Phys. Med. Rehabil.* **89**(9), 1693–1700 (2008).
36. R. Thorsen, L. Binda, S. Chiaramonte, D. Dalla Costa, T. Redaelli, E. Occhi, E. Beghi and M. Ferrarin, "Correlation among lesion level, muscle strength and hand function in cervical spinal cord injury," *Eur. J. Phys. Rehabil. Med.* (2013).
37. A. Kuppuswamy, A. Balasubramaniam, R. Maksimovic, C. Mathias, A. Gall, M. Craggs and P. Ellaway, "Action of 5hz repetitive transcranial magnetic stimulation on sensory, motor and autonomic function in human spinal cord injury," *Clin. Neurophysiol.* **122**(12), 2452–2461 (2011).
38. V. Mathiowetz, N. Kashman, G. Volland, K. Weber, M. Dowe, S. Rogers, *et al.*, "Grip and pinch strength: normative data for adults," *Arch. Phys. Med. Rehabil.* **66**(2), 69–74 (1985).
39. A. V. Berghe, M. Van Laere, S. Hellings and M. Vercauteren, "Reconstruction of the upper extremity in tetraplegia: Functional assessment, surgical procedures and rehabilitation," *Spinal Cord* **29**(2), 103–112 (1991).
40. L. Vaisman, L. Dipietro and H. I. Krebs, "A Comparative Analysis of Speed Profile Models for Wrist Pointing Movements ," *Proceedings of the IEEE Transactions on Neural Systems and Rehabilitation Engineering* (Dec. 2012) pp. 1–11.
41. T. Flash and N. Hogan, "The coordination of arm movements: an experimentally confirmed mathematical model," *J. Neurosci.* **5**(7), 1688–1703 (1985).
42. H. Beppu, M. Suda and R. Tanaka, "Analysis of cerebellar motor disorders by visually guided elbow tracking movement," *Brain***107**(3), 787–809 (1984).
43. B. Rohrer, S. Fasoli, H. I. Krebs, R. Hughes, B. Volpe, W. R. Frontera, J. Stein, and N. Hogan, "Movement smoothness changes during stroke recovery," *J. Neurosci.* **22**(18), 8297–8304 (2002).
44. P. Morasso, "Spatial control of arm movements," *Exp. Brain Res.* **42**(2), 223–227 (1981).
45. W. L. Nelson, "Physical principles for economies of skilled movements," *Biol. Cybern.* **46**(2), 135–147 (1983).
46. K. Takada, K. Yashiro and M. Takagi, "Reliability and sensitivity of jerk-cost measurement for evaluating irregularity of chewing jaw movements," *Physiol. Meas.* **27**(7), 609–622 (Apr. 2006).

47. N. Hogan and D. Sternad, "Sensitivity of smoothness measures to movement duration, amplitude and arrests," *J. Motor Behav.* **41**(6), 529–534 (2009).
48. F. Wilcoxon, "Individual comparisons by ranking methods," *Biometrics Bull.* **1**(6), 80–83 (1945).
49. J. H. van der Lee, R. C. Wagenaar, G. J. Lankhorst, T. W. Vogelaar, W. L. Devillé and L. M. Bouter, "Forced use of the upper extremity in chronic stroke patients results from a single-blind randomized clinical trial," *Stroke* **30**(11), 2369–2375 (1999).
50. R. G. Dong, J. Z. Wu, D. E. Welcome and T. W. McDowell, "A new approach to characterize grip force applied to a cylindrical handle," *Med. Eng. Phys.* **30**(1), 20–33 (Jan. 2008).
51. N. L. Tagliamonte, M. Scorcia, D. Formica, D. Campolo, and E. Guglielmelli, "Effects of impedance reduction of a robot for wrist rehabilitation on human motor strategies in healthy subjects during pointing tasks," *Adv. Robot.* **25**(5), 537–562 (2011).
52. Z. Kadivar, J. Sullivan, D. Eng, A. Pehlivan, M. O'Malley, N. Yozbatiran and G. Francisco, "Robotic Training and Kinematic Analysis of Arm and Hand After Incomplete Spinal Cord Injury: A Case Study," *2011 IEEE International Conference on Rehabilitation Robotics (ICORR)*. IEEE (2011) pp. 1–6.